Hindawi
Advances in Civil Engineering
Volume 2023, Article ID 8897139, 12 pages
https://doi.org/10.1155/2023/8897139

*Research Article*

# Measurement and Analysis of Deformation of Underlying Tunnel Induced by Foundation Pit Excavation

**Quan Yin,[1] Tan Xin ,[2] Hu Zhenggang,[2] and Huang Minghua[2]**

[1]*Hunan Engineering Research Center of Structural Safety and Disaster Prevention for Urban Underground Infrastructure, Hunan City University, Yiyang 413000, China*
[2]*Key Laboratory of Building Safety and Energy Conservation, Ministry of Education, Hunan University, Changsha 410082, China*

Correspondence should be addressed to Tan Xin; xintan@hnu.edu.cn

Received 28 July 2023; Revised 12 September 2023; Accepted 12 October 2023; Published 10 November 2023

Academic Editor: Cun Hui



The excavation of a foundation pit can exert a notable impact on the underlying tunnel. This research paper aims to analyze and synthesize measured deformation outcomes caused by foundation pit excavation on the underlying tunnel. The paper employs a two-stage analysis approach to derive the calculation formula for additional stress and the deformation control equation of the adjacent tunnel under the influence of foundation pit excavation. Subsequently, the Hermite spectrum method is applied to transform the deformation control equation of the underlying tunnel into a set of linear equations, enabling the determination of the deformation curve. To verify the precision of the theoretical calculation method, a comparative study is conducted between theoretical results and actual measurements. Moreover, a sensitivity analysis of crucial project factors is performed. The research findings reveal minimal disparity between theoretical calculation outcomes and measured deformation of the underlying tunnel, thus affirming the accuracy and rationality of the theoretical calculation formula. The excavation of the foundation pit leads to an uplift deformation in the underlying tunnel, resulting in an "n"-shaped deformation profile. Notably, the stiffness of the foundation soil and the depth at which the tunnel is buried emerge as pivotal factors influencing the deformation of the underlying tunnel. As the stiffness of the foundation soil and the depth of tunnel burial increase, the uplift deformation gradually diminishes, albeit within a restricted range of reduction.

## 1. Introduction

China's cities are currently undergoing rapid development, driven by the continuous expansion of domestic subway lines and urban infrastructure. Consequently, engineering construction activities in close proximity to established subway lines have become increasingly prevalent. In specific instances, the construction of new structures, such as underground complexes or high-rise buildings, demands extensive foundation pit excavations directly above existing subway tunnels. Unfortunately, such excavation efforts not only disrupt the integrity of these existing tunnels but also impact the surrounding soil. This impact results in a reduction in soil strength, giving rise to uneven deformations, leaks, segment cracking, and other related issues [1–3]. These complications pose a significant threat to the operational efficiency and safety of the tunnels. Thus, the study of vertical deformation in underlying tunnels, triggered by foundation pit excavation, carries immense practical significance, and holds potential for valuable applications [4–6].

At present, the research on the disturbance effect of foundation pit excavation is mainly divided into three aspects: model test, numerical simulation, and theoretical analysis. In terms of model test, Yu et al. [7] presented centrifugal model tests for excavation alongside existing tunnels in soft ground foundations. The bending moments of the diaphragm wall, ground settlement, tunnel deformation, and soil pressure around the tunnel are mainly investigated; Wang et al. [8] carried out centrifugal experiments on pit excavation and evaluated the tunnel deformation pattern and soil stress distribution between pit excavation and tunnel at different locations; Meng et al. [9] carried out three 3D centrifuge tests to investigate the response of the tunnel and ground due to nearby excavation in dry sand. Numerical simulations have

been a common calculation method used in civil engineering to predict construction-induced disturbances and risks. Zhao et al. [10] introduced the support structure for complex foundation pit projects, accumulating experience in the selection of support structures for similar projects. MIDAS/GTS software is used to establish a finite element model to evaluate the effect of excavation of different sections of the foundation pit on the tunnel deformation, and the accuracy of the finite element calculation results is verified by comparing the monitoring data; Xu et al. [11] presented a finite element parametric study of tunnel behavior caused by a nearby deep foundation excavation, analyzing the effects of tunnel location relative to the excavation, tunnel diameter, excavation dimensions, and tunnel protection measures on tunnel deformation. Shi et al. [12] studied the geometric effects of basement excavation on existing tunnels. The theoretical calculation method predicts disturbances caused by construction in a short period of time and uses a simple model that saves significantly on labor costs. Deng et al. [13] used the two-stage method to derive the formulae for calculating the deformation of a submerged tunnel triggered by the use of slope release excavation for the foundation pit and analyzed the effect of slope release factors on tunnel deformation. Based on Mindlin's displacement solution, Sun et al. [14] developed an analytical model for tunnel deformation due to circular excavation and verified the reliability of the solution by comparing it with the test results of existing centrifuge models and the analytical solution for square excavation. Cheng et al. [15] used a continuous Euler–Bernoulli beam to simulate shield tunnel behavior due to overlying basement excavation. However, the above studies regard the unloading stress in the process of foundation pit excavation as simply distributed additional load. In fact, the additional load generated after foundation pit excavation is relatively complex. In order to calculate the impact of complex additional load on adjacent tunnels after foundation pit excavation, Hermite spectrum method is introduced to assist the research. Hermite spectral method can solve differential equations, which is suitable for different forms of applied loads. It has fast convergence speed and high efficiency in the calculation process. At present, Hermite spectral method is rarely introduced into the related research of foundation pit excavation.

This paper introduces a theoretical calculation model, using Changsha Rail Transit Line 1 as a basis, to examine the impact of foundation pit excavation on underlying tunnels. The Mindlin solution is employed to calculate the additional stress at the axis of the underlying tunnel, taking into account the unloading of the foundation pit's side walls and bottom. Treating the underlying tunnel as an elastic beam on a Pasternak two-parameter foundation, a deformation control equation is formulated accordingly. To address this equation, the Hermite spectrum method is introduced, enabling the transformation of the deformation control equation into a system of linear algebraic equations. The resulting equations are then solved to derive the deformation curve of the underlying tunnel throughout the foundation pit excavation process. Furthermore, a sensitivity analysis of critical engineering parameters is conducted to pinpoint the parameters that exert the most influence on the real-world engineering scenario.

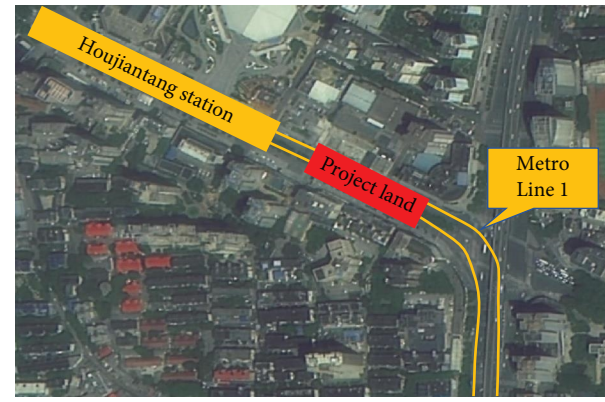


Figure 1: Geographical location of the project.

## 2. Automatic Monitoring of Foundation Pit Engineering

*2.1. Project Overview.* The current investigation is centered around an underground space development and construction endeavor, with the primary objective of establishing a linkage between Houjiatang Station of Changsha Rail Transit Line 1 and Tianhan Grand Theater. This project is strategically positioned in the northwest corner of the junction between Laodong Road and Furong Road, within the heart of Changsha's central urban region (see Figure 1). The project demands meticulous consideration of multiple intricate factors. Notably, the foundation pit floor of this undertaking lies in close proximity to the tunnel roof of Changsha Line 1, while the rail tunnels themselves are positioned directly beneath the foundation pit, extending in the southern direction. Importantly, the ongoing construction of Line 1 has been in progress since 2016. It is imperative to recognize that the excavation of the foundation pit will induce a reduction in overlying burden on the crown of the Line 1 tunnel. This reduction has the potential to disrupt the equilibrium between upper and lower stresses within the tunnel, ultimately causing an uplift in the shield tunnel and imposing supplementary stress on the tunnel segment. As a result, the operational safety of the entire system could be compromised.

The project's foundation pit area assumes an approximately rectangular shape, measuring around 89 m in length and 43–53 m in width. The basement floor boasts a thickness of $h = 1{,}200$ mm, while the cushion exhibits a thickness of $h = 100$ mm. The prevailing ground elevation stands between 60.00 and 65.50 m, with the basement floor's bottom elevation situated at 55.30 m. The foundation pit's excavation reaches a depth of 54.00 m. Preceding the commencement of foundation pit construction, the terrain is leveled to an elevation not surpassing 65.40 m. The targeted depth for the foundation pit is set at 5.8–10.3 m. The foundation pit's support system encompasses a combination of bite piles and anchor cables, reinforced by internal support mechanisms. To mitigate adverse effects on the underlying tunnel, grouting is employed to seal the bottom portion.

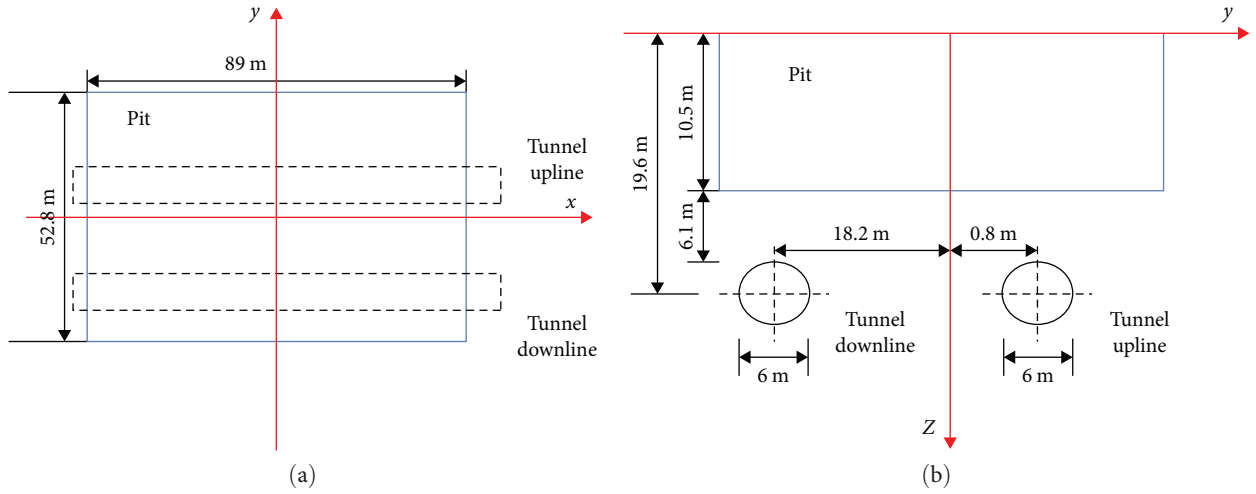


Figure 2: Schematic diagram of relative position between foundation pit and tunnel. (a) Foundation pit tunnel plan. (b) Elevation of foundation pit tunnel.

Table 1: Values of design parameters for each formation.

| Formation | Layer thickness (m) | Natural gravity (kN/m$^3$) | Compression modulus (MPa) | Cohesion (kPa) | Internal friction angle (°) | Average thickness (m) |
|---|---|---|---|---|---|---|
| Artificial fill | 3.2 | 18.8 | 2.5 | 10 | 10 | 2 |
| Silty clay | 3.6 | 19.8 | 8 | 30 | 20 | 3 |
| Coarse sand | 1.1 | 20.5 | 25 | 4 | 32 | 6 |
| Round gravel | 2.8 | 21.0 | 35 | 3 | 35 | 2 |
| Pebble | 2.1 | 21.0 | 40 | 1 | 40 | 7 |
| Strongly weathered argillaceous siltstone | 8.1 | 23.1 | – | – | – | 13 |
| Moderately weathered argillaceous siltstone | 3.6 | 24.1 | – | – | – | – |

Rail Track Line 1 is representative of a standard shield tunnel, featuring an outer diameter of 6 m and a lining thickness of 0.3 m. The minimum distance between the foundation pit's bottom plate and the top plate of Track Line 1 amounts to 6.1 m. This tunnel predominantly traverses the intensely weathered argillaceous silty rock stratum. The tunnel's upper and lower lines exhibit near-parallel alignment with the longer side of the foundation pit. Specifically, the upper line maintains a proximity of 0.8 m from the foundation pit's center, whereas the lower line is positioned 18.2 m away from the center. The horizontal spacing between the tunnel's upper and lower lines measures 19 m. Refer Figure 2 for an illustrative representation of the foundation pit and tunnel's relative positioning.

See Table 1 for basic information and relevant parameters of soil layer within the scope of the project.

*2.2. Automatic Monitoring Scheme.* The monitoring initiative for the supporting project encompasses two specific mileage sections: ydk20 + 780–ydk20 + 920 and zdk20 + 780–zdk20 + 920, both integral parts of Rail Transit Line 1. This monitoring campaign encompasses the Houjiatang Nanhu Road section of the line as well as the platform layer of Houjiatang Station. The primary objective of this monitoring effort is to evaluate the deformation within the underlying section of the line throughout the process of foundation pit excavation. Simultaneously, the aim is to ensure the uninterrupted operational integrity of the existing subway tunnel.

The extent of monitoring for this project is delineated as follows: The tunnel section is subjected to monitoring within a 30-m range, spanning from the sideline adjacent to the foundation pit. This selection results in an aggregated length of approximately 140 m. To comprehensively cover the influence zones, automatic monitoring segments are strategically positioned at intervals of 5 m within the primary influence region, and at intervals of 10 m within the secondary influence zone. In the context of each tunnel, an individual automatic measurement robot is deployed, summing up to a collective deployment of two robots. This configuration results in a total of 24 sections per tunnel and an overall aggregate of 48 sections. The layout of the monitoring sites is shown in Figure 3.

*2.3. Analysis of Monitoring Results.* Monitoring activities were conducted within specific timeframes related to the project's construction. From January 11, 2018, which marked the commencement of construction to April 15, 2019, the conclusion of the roof construction, encompassed the construction phase monitoring. Subsequently, during the stability

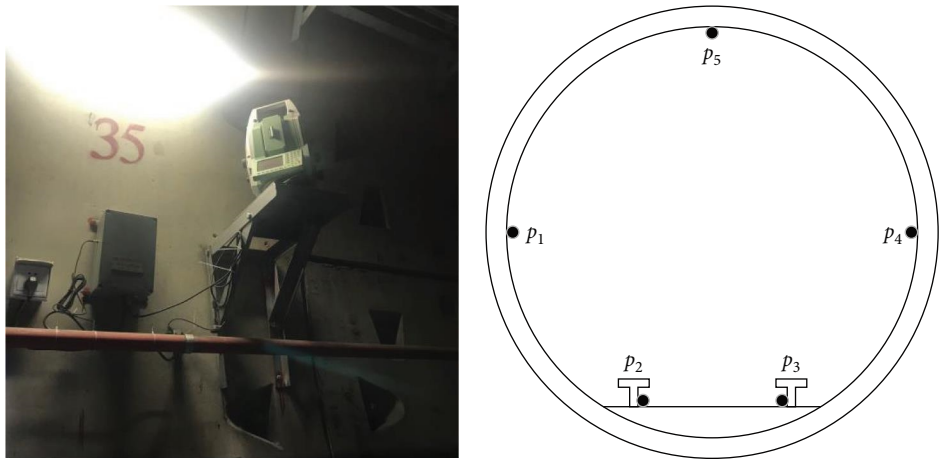


(a) (b)

Figure 3: Schematic diagram of automatic monitoring points. (a) Layout of monitoring points. (b) Location of monitoring points.

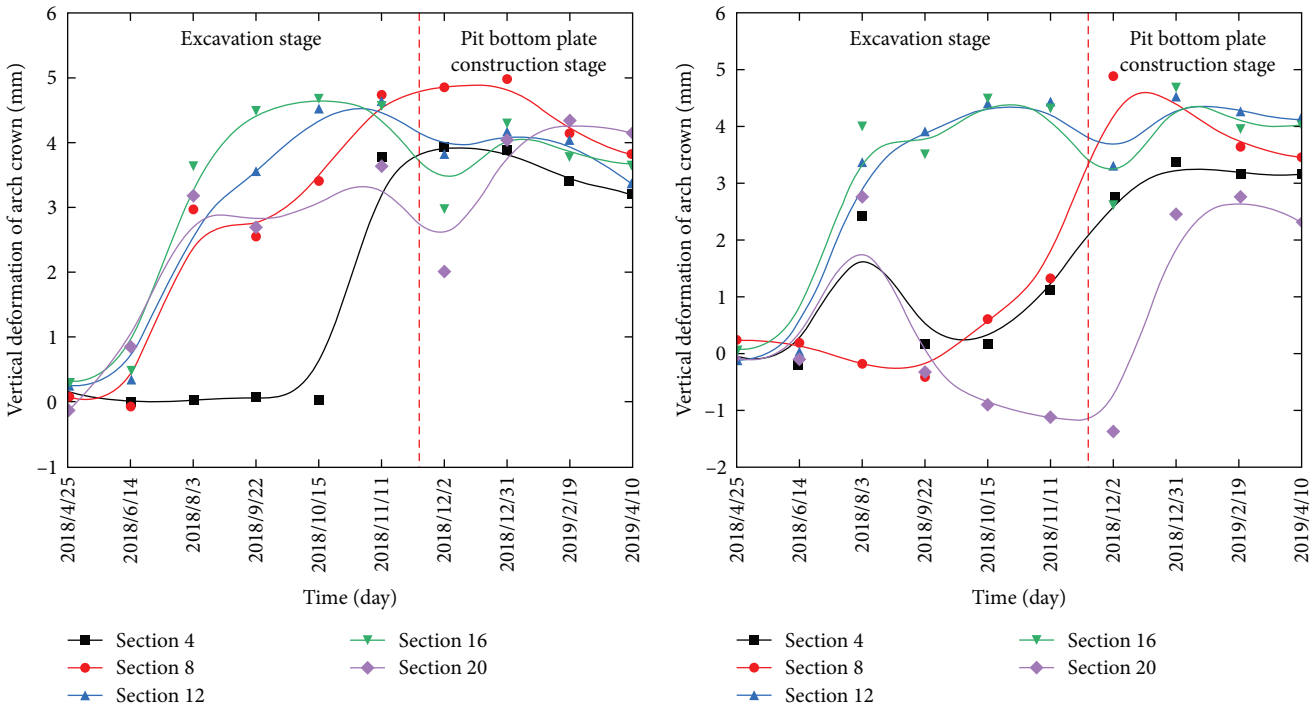


(a) (b)

Figure 4: Automated monitoring results. (a) Upward tunnel. (b) Downward tunnel.

period, monitoring occurred from January 11, 2019 (following the bottom plate's completion) until April 21, 2019 (the final capping of the foundation pit).

Throughout the foundation pit excavation and the bottom slab's construction, the tunnel structure of Line 1 exhibited a discernible degree of uplift. Figure 4 visually presents the vertical deformation curve of the arch crown for specific sections (4, 8, 12, 16, and 20) of the uplink tunnel. Notably, sections 8, 12, and 16 are tunnel segments positioned in closer proximity to the foundation pit's center, while sections 4 and 20 are more distantly situated.

Analysis of Figure 4 reveals that as the excavation depth of the foundation pit progressed, the vertical deformation of the arch crown in various tunnel sections concurrently increased. Generally, tunnel segments in closer proximity to the foundation pit's center (sections 8, 12, and 16) exhibited more pronounced vertical deformation in comparison to those situated farther away (sections 4 and 20). This observed variation is a direct consequence of the heightened influence of the foundation pit excavation closer to its center.

Moreover, it is worth noting that the vertical deformation of the arch crown within each tunnel section did not follow a

Table 2: Deformation monitoring results for the lower recumbent tunnel.

| Maximum uplift | November 27, 2018 | The bottom plate was completed on January 11, 2019 | Top plate completed on April 21, 2019 | 100 days after completion of the base plate | | Control value (mm) |
|---|---|---|---|---|---|---|
| | Accumulated displacement (mm) | Accumulated displacement (mm) | Accumulated displacement (mm) | Deformation value (mm) | Deformation rate (mm/day) | |
| Upward tunnel | 5.09 | 4.46 | 3.71 | −0.75 | −0.008 | 7 |
| Downward tunnel | 5.13 | 4.46 | 3.85 | −0.61 | −0.006 | 7 |

linear progression over time; instead, it displayed a tendency of decline throughout the process. This behavior can be attributed to the deployment of support structures and anchor cables within the foundation pit at distinct excavation stages. As the foundation pit floor was constructed, the vertical deformation of the arch crown in each tunnel section gradually diminished to varying degrees, ultimately converging toward stability. This trend is primarily due to the mitigating effect exerted by the foundation pit floor and its structural elements on the uplift deformation experienced by the existing tunnel beneath.

By meticulously scrutinizing the monitoring data collected over a stable period of almost 100 days following the finalization of the bottom plate construction, the outcomes are succinctly summarized in Table 2. The data showcases that the highest rate of elevation displacement change (−0.012 mm/day) aligns harmoniously with the parameters outlined in the "Code for Building Deformation Measurement (China)" (JGJ8-2016) which prescribes a range of 0.01–0.04 mm/day. This correspondence underscores that the observed deformation remains well within the prescribed acceptable limits. Furthermore, it is discernible that the deformation tendencies tend to stabilize as time progresses.

Throughout the foundation pit construction connecting Houjiatang Station and Tianhan Grand Theater, the deformation values detected within the underlying tunnel, for each monitored parameter, exhibited relative modesty. Equally significant, the cumulative deformation values and deformation rates consistently adhered to permissible thresholds. These ascertainments distinctly affirm that the track section maintained a secure and manageable condition.

## 3. Additional Stress in Soil Caused by Excavation of Foundation Pit

*3.1. Theoretical Calculation Assumptions.* The influence of soil stratification was not considered in this paper. Hirai [16] established the theory of the equivalent layered method. This method of soil layer homogenization is widely used to calculate the nonuniform distribution of soil layers [17, 18], so this paper uses the same method to deal with the unevenly distributed soil layer. The conversion formula is given as follows:

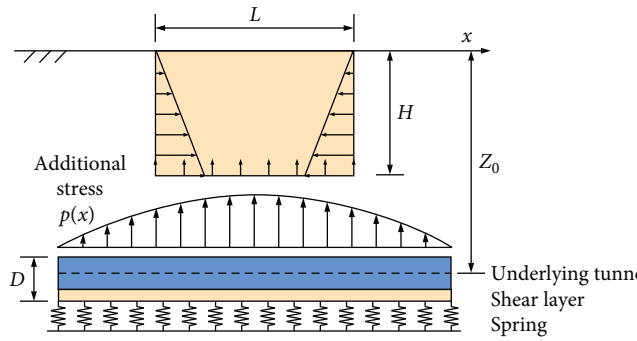


Figure 5: Mechanical analysis model of underlying tunnel.

$$H_{je} = \begin{cases} \left[\dfrac{E_j(1-\mu_n{}^2)}{E_n(1-\mu_j{}^2)}\right]^{1/3} H_j, E_j > {}_n \\ \left(\dfrac{3}{4} + \dfrac{1}{4}\left[\dfrac{E_j(1-\mu_n{}^2)}{E_n(1-\mu_j{}^2)}\right]^{1/3}\right) H_j, E_j \le E_n \end{cases}, \quad (1)$$

where $j$ is the number of the soil layer, $1 \le j \le n$; $E_j$ is the elastic modulus of layer soil $j$, $\mu_j$ is the Poisson's ratio of layer soil $j$, $H_j$ is the actual thickness of $j$th layer, $H_{je}$ is the equivalent thickness of $j$th layer, $En$ is the elastic modulus for $n$th layer (base soil layer), and $\mu_n$ is the Poisson's ratio for $n$th layer (base soil layer).

This paper does not consider the effect of pit precipitation and peripheral additional stresses on existing tunnels and only considers the deformation of tunnels triggered by the pit excavation process.

*3.2. Computation Model.* The excavation of foundation pits invariably exerts an impact on the underlying tunnel, leading to the emergence of supplementary stress and deformation within the tunnel. To effectively compute this additional stress and deformation experienced by the underlying tunnel, a comprehensive calculation model is devised, as visually represented in Figure 5. Given the close proximity existing between the upstream tunnel and the foundation pit's centerline, the focal analysis within the depicted calculation model, as depicted in Figure 5, pertains to the stress and deformation dynamics of the upstream tunnel. In the context of Figure 5, the parameters $L$ and $H$ symbolize the

foundation pit's length and height, respectively. The variable $Z_0$ denotes the depth at which the centerline of the underlying tunnel is situated below the surface, while $D$ characterizes the diameter of the underlying tunnel. The intricate interplay between the tunnel and its encompassing soil is elegantly captured through the application of the Pasternak dual-parameter model [19–21].

*3.3. Additional Stress Caused by Unloading at the Bottom of the Foundation Pit.* The Mindlin solution [22] can be used to calculate the additional stress under the influence of excavation unloading of the foundation pit. Assuming that the unit force at any point at the bottom of the foundation pit is $p_1 dxdy$, the vertical additional stress of the underlying tunnel caused by excavation unloading of the foundation pit bottom is given as follows:

$$p_1(x) = \int_{-\frac{L}{2}}^{\frac{L}{2}} \int_{-\frac{B}{2}}^{\frac{B}{2}} \frac{p_1 dxdy}{8\pi(1-\mu)} \left[ \frac{(1-2\mu)(z_0-H)}{R_1^3} + \frac{3(z_0-H)^3}{R_1^5} - \frac{(1-2\mu)(z_0-H)}{R_2^3} + \frac{3z_0(3-4\mu)(z_0+H)^2}{R_2^5} - \frac{3H(z_0+H)(5z_0-H)}{R_2^5} + \frac{30Hz_0(z_0+H)^3}{R_2^7} \right], \tag{2}$$

where $B$ is the width of the pit,
$R_1 = \sqrt{(x-X)^2 + (y_0-Y)^2 + (z_0-H)^2}$ ,
$R_2 = \sqrt{(x-X)^2 + (y_0-Y)^2 + (z_0+H)^2}$,
$\mu$ is the Poisson 's ratio of soil, $(X, Y, Z)$ are the coordinates of the calculation points at the bottom of the foundation pit, and $(x, y_0, z_0)$ are the coordinates of the stress points of the axis of the underlying tunnel.

*3.4. Additional Stress Caused by Unloading of Foundation Pit Sidewall.* In the process of foundation pit excavation, in addition to the additional stress generated by the unloading of the bottom of the foundation pit, the unloading of the side wall of the foundation pit will also produce additional stress. As shown in Figure 5, the unloading stress generated by the excavation of the side wall of the foundation pit is triangularly distributed, and its size is $K_0\gamma z$ ($K_0$ is the coefficient of static earth pressure). Assuming that the unit force at any point on the left side wall of the foundation pit is $p_2 dydz$ ($p_2 = K_0\gamma z$), the vertical additional stress of the underlying tunnel caused by the excavation and unloading of the left side wall of the foundation pit is given as follows:

$$p_2(x) = \int_{-\frac{B}{2}}^{\frac{B}{2}} \int_0^H \frac{p_2 dydz}{8\pi(1-\mu)} \left[ -\frac{(1-2\mu)z}{T_1^3} + \frac{(1-2\mu)z}{T_2^3} + \frac{3(z_0-H)^3}{T_1^5} + \frac{3z(3-4\mu)(z_0+z)^2}{T_2^5} - \frac{3z(z_0+z)(5z_0-z)}{T_2^5} + \frac{30z_0z^2(z_0+z)^3}{T_2^7} \right], \tag{3}$$

where $T_1 = \sqrt{(x-L/2)^2 + (y_0-Y)^2 + (z_0-Z)^2}$ and $T_2 = \sqrt{(x-L/2)^2 + (y_0-Y)^2 + (z_0+Z)^2}$. The pressure coefficient of static soil is generally obtained by field test or empirical formula, which is used in this paper.

In sandy soil, the pressure coefficient of static soil is given as follows:

$$K_0 = 1 - \sin\varphi \,, \tag{4}$$

where $\varphi$ is the internal friction angle of soil.

In clay, the pressure coefficient of static soil is [23–25] given as follows:

$$K_0 = 0.95 - \sin\varphi \,. \tag{5}$$

In overconsolidated soil, the pressure coefficient of static soil is given as follows:

$$K_0 = \mathrm{OCR}(1 - \sin\varphi) \,, \tag{6}$$

where OCR is the overconsolidation ratio of the soil mass.

In addition to the additional stress generated by the bottom and left side walls of the foundation pit at the axis of the underlying tunnel, the right, front, and rear side walls of the foundation pit also generate additional stress at the axis of the underlying tunnel. Similarly, the vertical additional stresses $p_3(x)$, $p_4(x)$, and $p_5(x)$ generated by the right, front, and rear side walls of the foundation pit at the axis of the underlying tunnel can be solved according to Equation (3). The additional stress generated by excavation and unloading at all positions of the foundation pit is superimposed to obtain the additional stress generated by excavation at the axis of the underlying tunnel as follows:

$$p(x) = p_1(x) + p_2(x) + p_3(x) + p_4(x) + p_5(x) \,. \tag{7}$$

## 4. Tunnel Deformation Caused by Excavation of Foundation Pit

*4.1. Tunnel Deformation Control Equation.* In the calculation model shown in Figure 5, the underlying tunnel can be considered as an elastic foundation beam placed on the Pasternak foundation. For the Pasternak foundation beam model, there is a relationship between the deformation of the underlying tunnel and the surrounding foundation soil [26–28]:

$$q(x) = kw(x) - G\frac{d^2w(x)}{dx^2}, \tag{8}$$

where $q(x)$ is the foundation reaction force, $K$ is the coefficient of the foundation bed, $k = \frac{1.3E_S}{D(1-\mu^2)}\sqrt[12]{\frac{E_sD^4}{E_tI_t}}$, $E_s$ is the elastic modulus of the foundation soil and is the equivalent bending stiffness of the tunnel, $w(x)$ is the displacement of the foundation soil, and $G$ is the shear stiffness of the soil around the tunnel. The shear stiffness of the soil around the tunnel can be calculated according to the following formula [29, 30]:

$$G = \frac{E_sh_s}{6(1+\mu)}\ , \tag{9}$$

where $h_s$ is the thickness of the monitoring layer, $h_s = 2.5D$.

According to the Euler–Bernoulli beam theory, the relationship between the vertical displacement $w(x)$ of the underlying tunnel and its additional stress $p(x)$ and the foundation reaction $q(x)$ satisfies the following equation:

$$\mathrm{EI}\frac{d^4w(x)}{dx^4} = D[p(x) - q(x)]\ . \tag{10}$$

Substituting Equation (8) into Equation (10), it can be obtained that the vertical deformation of the underlying tunnel satisfies the following Equation (11):

$$\mathrm{EI}\frac{d^4w(x)}{dx^4} - GD\frac{d^2w(x)}{dx^2} + kDw(x) = Dp(x)\ . \tag{11}$$

*4.2. Hermite Spectral Solution for Tunnel Deformation.* Prominent scholars in the field suggest that researchers can effectively employ the Hermite spectral analysis method to convert the deformation control equation of the underlying tunnel into a set of linear algebraic equations. When measured against alternative techniques like the Lagrange interpolation method and the Newton interpolation method, the Hermite spectral approach impeccably addresses two vital requisites. Specifically, it ensures that the value of the interpolating function at the interpolation point coincides with the function's value. Furthermore, it guarantees that the derivative of the interpolating function at the interpolation point matches the derivative of the function, or adheres to specific predetermined constraints. As a direct consequence of these intrinsic characteristics, the Hermite spectral method emerges as a notably superior option in terms of accuracy when juxtaposed with the other two methodologies. The expression for the Hermite function [31] is given as follows:

$$\widehat{H}_n(\xi) = \frac{1}{\pi^{1/4}\sqrt{2^n n!}}H_n(\xi),\ n \geq 0, \tag{12}$$

where $H_n(\xi)$ is an $n$-order Hermite polynomial. For any function $\Psi(\xi)$, the finite term Hermite function can be used to expand this function, and the expanded function expression is given as follows:

$$\psi(\xi) = \sum_{n=0}^{N-1}\widetilde{\psi}(\xi)\widehat{H}_n(\xi), \tag{13}$$

where $\tilde{\psi}(\xi)$ is the function of $\Psi(\xi)$. The coefficient of the $n$-order Hermite function expansion, $\tilde{\psi}(\xi)$, is expressed as follows:

$$\widetilde{\psi}_n = \sum_{j=0}^{N-1}\psi(\xi_j)\widehat{H}_n(\xi_j)\widehat{\omega}_j,\ \ 0 \leq n \leq N. \tag{14}$$

where $\xi_j$ is the zero point of the Hermite function, $\widehat{\omega}_j$ is the corresponding weight, and the expression for $\widehat{\omega}_j$ is given as follows:

$$\widehat{\omega}_j = \frac{1}{N\widehat{H}_{N-1}^2(\xi_j)},\ \ 0 \leq j \leq N-1. \tag{15}$$

According to the Hermite function, let $\xi = \beta^{-1}x$, $u(\xi) = w(x)$, $\rho(\xi) = p(x)$, substituting it into Equation (11), we obtain the new downward tunnel deformation control equation as follows:

$$\frac{\mathrm{EI}}{D\beta^4}\frac{d^4u(\xi)}{d\xi^4} - \frac{G}{\beta^2}\frac{d^2u(\xi)}{d\xi^2} + ku(\xi) = \rho(\xi)\ , \tag{16}$$

where $u(\xi)$ and $\rho(\xi)$ can be calculated using the Hermite function for expansion and the specific expression after expansion is given as follows:

$$u(\xi) = \sum_{n=0}^{N-1}\widetilde{u}(\xi)\widehat{H}_n(\xi), \rho(\xi) = \sum_{n=0}^{N-1}\widetilde{\rho}(\xi)\widehat{H}_n(\xi)\ , \tag{17}$$

$\tilde{u}(\xi)$ and $\tilde{\rho}(\xi)$ can be solved by referring to Equation (14). Equations (15) and (17) can be rewritten as a system of linear equations from Equations (14) and (17):

$$\frac{\mathrm{EI}}{D\beta^4}\boldsymbol{D}^4\boldsymbol{u} - \frac{G}{\beta^2}\boldsymbol{D}^2\boldsymbol{u} + k\boldsymbol{u} = \rho, \tag{18}$$

where $\boldsymbol{u} = \{u(\xi_0),\ u(\xi_1)\cdots,\ u(\xi_{N-1})\}^T$和 $\rho = \{\rho(\xi_0),\ \rho(\xi_1)\cdots,\ \rho(\xi_{N-1})\}^T$.

Table 3: Theoretical calculation parameter values.

| $L$ | $B$ | $Z_0$ | $D$ | $\mu$ |
|---|---|---|---|---|
| 89 m | 53 m | 16.6 m | 6 m | 0.35 |
| $\gamma$ | $\varphi$ | $G$ | $EI$ | |
| 19.7 kN/m$^3$ | 23° | 36.4 MPa | $7.8 \times 10^4$ MN m$^2$ | |

The answer to Equation (18) is given as follows:

$$\boldsymbol{u} = \left(\frac{\mathrm{EI}}{D\beta^4}\boldsymbol{D}^4 - \frac{G}{\beta^2}\boldsymbol{D}^2 + k\boldsymbol{I}\right)^{-1}\rho, \tag{19}$$

where $\boldsymbol{I}$ is the identity matrix.

## 5. Engineering Case Verification

In this section, the Hermite spectral method is employed to determine the theoretical vertical deformation of the existing tunnel resulting from the excavation of the foundation pit in the engineering case. The Hermite spectral solution is validated and compared against the measured data, with the following calculation parameters:

The foundation pit has dimensions of 89 m × 53 m, with a rectangular shape.

The excavation depth of the foundation pit is 10.5 m.

The outer diameter of the existing tunnel is 6 m, representing a typical shield tunnel.

The tunnel axis is parallel to the long side of the foundation pit.

The top plate of the tunnel is situated 6.1 m above the bottom plate of the foundation pit.

The buried depth of the tunnel axis is 19.6 m.

The distance from the upward line of the tunnel to the center of the foundation pit is 0.8 m, while the downward line is parallel to the upward line and located 18.2 m away from the center of the foundation pit.

The bending stiffness of the tunnel is equivalent to $7.8 \times 10^4$ MN · m$^2$.

The equivalent weight of the soil is 19.7 kN/m$^3$.

The Poisson's ratio is assumed to be 0.35.

The existing tunnel is situated in strongly weathered argillaceous siltstone.

A 3-m thick grouting reinforcement area is present in the soil below the foundation pit floor.

The interaction between the underlying tunnel and the foundation soil is characterized using the Pasternak model.

Considering the improvement of the foundation, the elastic modulus of the soil is taken as 60 MPa.

Summarizing the above parameters, the parameters used in the theoretical formulation are shown in Table 3.

To holistically evaluate the comprehensive impact of the entire foundation pit excavation process on the vertical deformation of the preexisting tunnel, the theoretical calculation incorporates a linear progression in foundation pit depth, commencing from a foundational depth of 1.5 m. Commencing from the initiation of the project on January 11, 2018, the excavation of the foundation pit reached a depth of 1.5 m by May 20, 2018. By September 1, 2018, the excavation's depth extended to 7.5 m, ultimately culminating in the full excavation completion on November 27, 2018. Figure 6 graphically depicts the theoretical values of vertical deformation within the upward tunnel line at varying excavation depths, alongside measured deformation values collected during three distinct periods. The observed trend underscores the alignment between theoretical calculation results and measured data for excavation depths of 1.5 and 7.5 m. While a slight elevation in the theoretical calculation results compared to the measured data is discernible, this discrepancy remains relatively minor. Upon the conclusion of the foundation pit excavation, the theoretical calculation indicates a peak vertical deformation of 6.39 mm. Conversely, the measured data registers a maximum vertical deformation of 5.14 mm, thereby establishing a difference of 19.56% between the two sets of data.

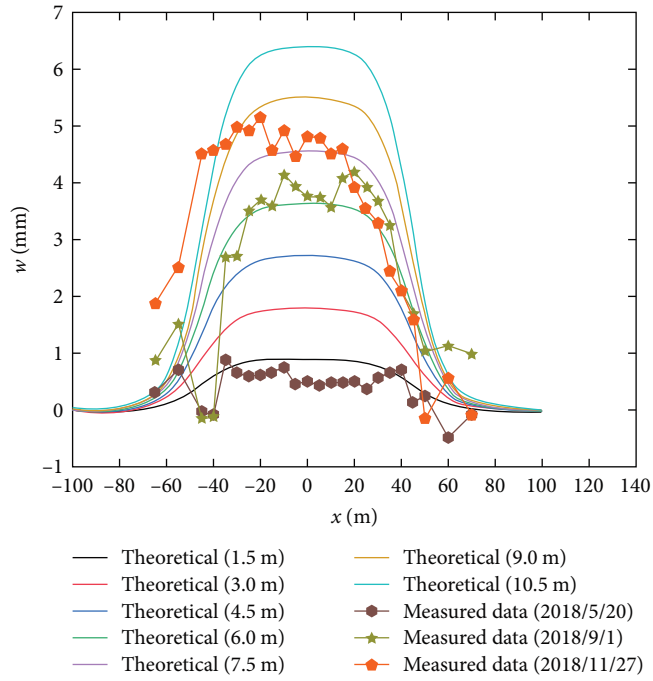


Figure 6: Comparison of vertical deformation results of tunnel upstream line.

This disparity between theoretical calculation and measured values can be attributed to several contributing factors. First, theoretical calculations often incorporate simplified conditions and overlook practical influences, such as enclosure structures and soil reinforcement, on vertical deformation within existing tunnels. Furthermore, a notable 3-m thick grouting reinforcement zone exists in the upper section of the existing tunnel, substantially alleviating vertical deformation. Finally, the practical application of pouring the bottom plate postfoundation pit excavation also plays a pivotal

role in minimizing vertical deformation in the existing tunnel. Despite these variations, the overarching trend of alterations within the upward tunnel line demonstrates a commendable consistency between theoretical calculations and measured data. Additionally, it is important to underscore that the theoretical calculation outcomes remain below the designated tunnel uplift control threshold of 7 mm, a significant affirmation. In summary, the theoretical calculation results exhibit a gratifying level of correspondence with measured data and persistently uphold the established tunnel uplift control value. It is imperative to acknowledge that while the theoretical calculation may exclude certain practical elements, it nevertheless yields invaluable insights into the vertical deformation of the existing tunnel during foundation pit excavation.

## 6. Parameter Analysis

In order to thoroughly evaluate the influence of diverse construction factors on the deformation of the underlying tunnel within practical engineering contexts, the calculation scenario depicted in Figure 6 serves as the foundational reference. In this analytical endeavor, each parameter encompassed by this reference scenario is independently manipulated to explore its individual impact on the deformation of the underlying tunnel. This systematic parameter variation facilitates a comprehensive investigation of the tunnel's deformation across diverse scenarios. Through this meticulous analysis involving parameter adjustments, the deformation exhibited by the underlying tunnel is examined under distinct circumstances. This detailed examination empowers a holistic comprehension of the manner in which each parameter wields influence over the tunnel's deformation. As a result, this analytical approach furnishes invaluable insights into engineering design and construction practices by elucidating the nuanced impacts of each parameter on tunnel deformation.

*6.1. Foundation Soil Stiffness.* In order to dissect the impact of foundation soil stiffness on the deformation of the underlying tunnel, the stiffness of the foundation soil is strategically selected as the controlled variable. In particular, the elastic modulus of the foundation soil ($E_s$) is varied across values of 30, 40, 50, 60, and 70 MPa. Figure 7 visually portrays the resultant tunnel deformation for distinct foundation soil stiffness scenarios.

Figure 7 conveys a clear depiction of the vertical deformation pattern exhibited within the subterranean tunnel, predominantly situated beneath the foundation pit. The most notable vertical deformation is directly beneath the foundation pit's centerline. Importantly, the perturbation and deformation triggered by foundation pit excavation remain confined within an approximate radius of 60 m from the centerline of the foundation pit. As a direct consequence of the foundation pit excavation's influence, the underlying tunnel's deformation takes on an evident upward uplift deformation pattern. Moving progressively away from the foundation pit's centerline, the vertical deformation of the underlying tunnel gradually approaches a null value. The interplay between foundation pit excavation and the

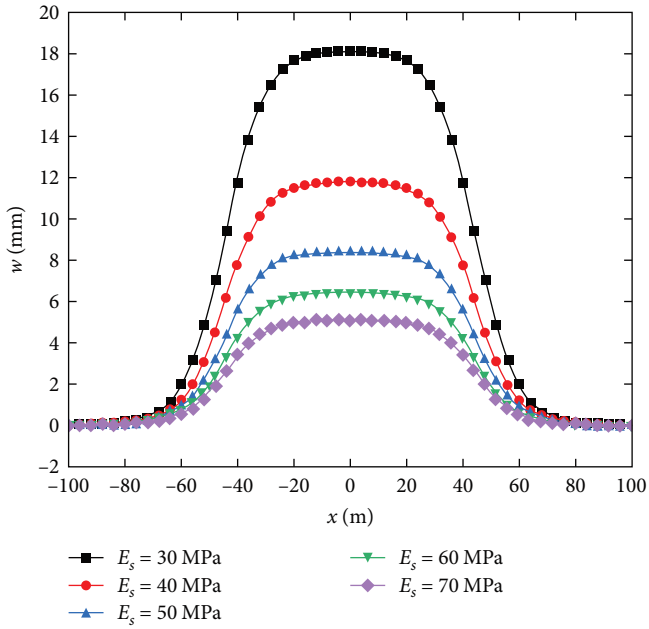


Figure 7: Influence of stiffness value of foundation soil.

underlying tunnel deformation produces a noteworthy trend. With increasing distance from the foundation pit's centerline, the vertical deformation of the underlying tunnel tends to diminish. This trend is further accentuated by the rise in stiffness of the foundation soil. The heightened stiffness translates to the foundation soil exhibiting a heightened resistance to deformation. This enhanced resistance corresponds to reduced vertical deformations within the foundation soil, at comparable stress levels, consequently resulting in the mitigation of vertical deformations within the underlying tunnel.

*6.2. Tunnel Burial Depth.* To thoroughly evaluate the impact of the buried depth of the lower lying tunnel on tunnel deformation, the buried depth itself is systematically manipulated as the controlled variable. This analysis encompasses a spectrum of tunnel buried depths: $h = 6$, 9, 12, 15, and 18 m. The resulting tunnel deformation under these varying conditions is succinctly presented in Figure 8.

Figure 8 offers insightful observations regarding the deformation characteristics of the underlying tunnel. A notable symmetry is observed in the deformation curve along the centerline of the foundation pit ($x = 0$ m). The deformation pattern exhibited by the underlying tunnel materializes as an upward uplift deformation, distinctly resembling the shape of the letter "n." Remarkably, the highest point on this "n" deformation curve coincides with $x = 0$ m, which corresponds to the direct alignment beneath the foundation pit's centerline.

Furthermore, the investigation uncovers that as the buried depth of the underlying tunnel increases, the extent of the tunnel's deformation progressively diminishes. This diminishing deformation magnitude is accompanied by a reduction in the rate of deformation reduction. Notably, the width of the elevated arch, characterized by the "n" shape, contracts

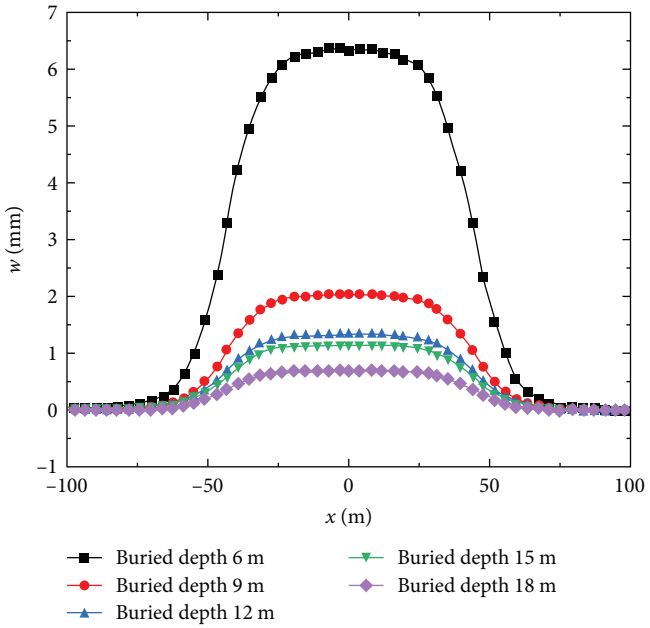


Figure 8: Impact of tunnel roof burial depth.

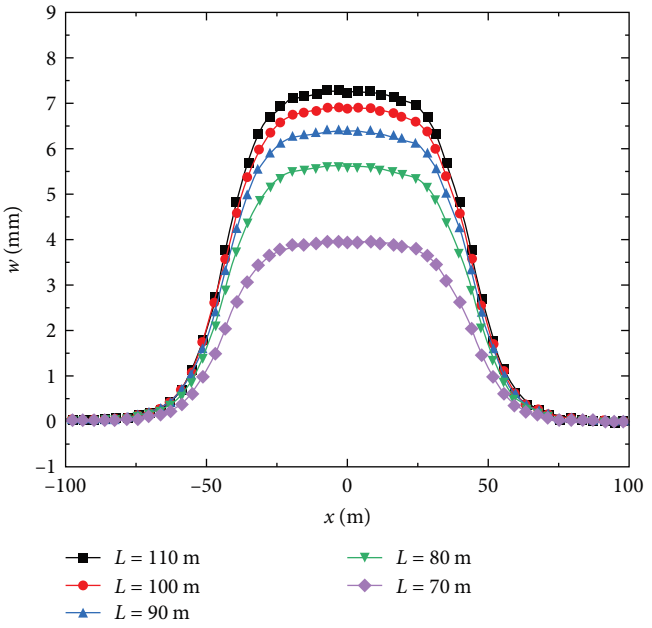


Figure 9: Impact of foundation pit length.

in tandem with the increase in burial depth. This phenomenon arises from the gradual attenuation of the disruptive effects originating from foundation pit excavation, as the distance between the tunnel and the foundation pit augments. As the buried depth of the underlying tunnel escalates, the spatial separation between the tunnel and the foundation pit amplifies. Consequently, the disruptive influence experienced by the underlying tunnel experiences gradual attenuation, thereby precipitating a progressive reduction in tunnel deformation.

*6.3. Excavation Size of Foundation Pit.* In order to comprehensively evaluate the ramifications of foundation pit excavation size, two pivotal factors are diligently considered: the length ($L$) and width ($B$) of the excavation. With focused precision, the foundation pit excavation size assumes the role of the controlled variable. Within this investigative framework, the length of excavation spans a range of 70–110 m, while the excavation width extends across a spectrum of 20–50 m. The ensuing deformation curves delineating the impact on the underlying tunnel for varying analysis conditions are thoughtfully depicted in Figures 9 and 10.

Upon perusal of Figures 9 and 10, a discernible trend emerges: the vertical displacement of the underlying tunnel mirrors the variations in both length and width of the foundation pit excavation. Notably, the effect stemming from the length of the foundation pit assumes a more pronounced significance. This distinction can be attributed to the pivotal role played by the foundation pit's dimensions. As the dimensions of the foundation pit excavation augment, the associated disruption stemming from excavation extends across a broader expanse. This extended disruption amplifies

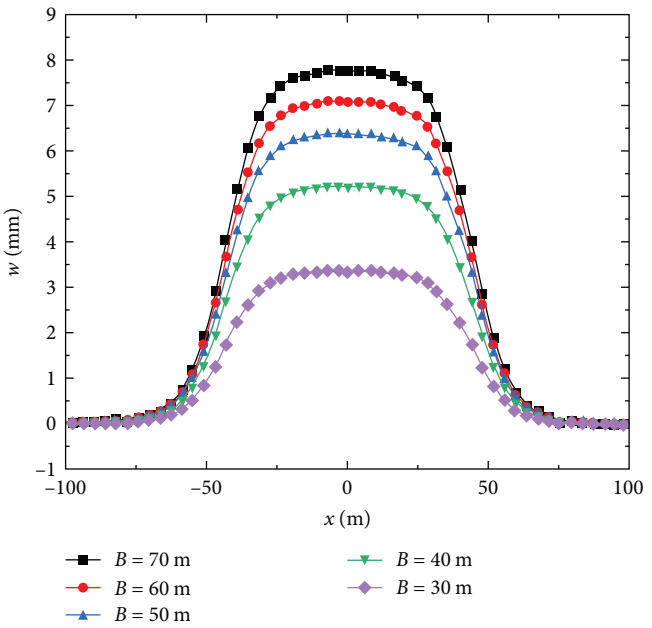


Figure 10: Impact of foundation pit width.

the overall impact, consequently precipitating greater deformation within the underlying tunnel.

In light of these insightful conclusions, the imperative to manage the extent of disruption originating from foundation pit excavation during the actual process becomes unmistakably evident. Navigating this scenario adeptly necessitates an artful balance, as efforts to control the dimensions of the excavation serve the pivotal purpose of

minimizing the extent of influence on the underlying tunnel's deformation.

## 7. Conclusion

In this paper, a comprehensive analysis is undertaken based on the two-stage method and Hermite spectrum method. This analysis leads to the derivation of a deformation calculation formula, specifically addressing the deformation caused by the undercut tunnel bulge induced by foundation pit excavation. The derived formula is then meticulously compared against actual monitoring data to substantiate the method's viability and the theoretical prediction formula's rationality. Ultimately, the study delves into the exploration of design parameters' influence on tunnel deformation, culminating in the following conclusive findings:

(1) Upon the culmination of foundation pit excavation, the theoretical calculation yields a maximum vertical deformation of 6.39 mm. Contrastingly, the measured data reveal a maximum vertical deformation of 5.14 mm, indicating a discernible difference of 19.56% between the two sets of data. This variance, however, serves to affirm the precision and logical soundness of the employed calculation method. Furthermore, the proposed calculation methodology exhibits particular relevance in scenarios involving external loads, furnishing fresh perspectives for the exploration of excavation effects on proximate structures.

(2) The research discoveries uncover a noteworthy pattern: The disruptive deformation range instigated by foundation pit excavation engulfs an approximate span of 60 m from the centerline of the foundation pit. This disruption's zenith manifests directly beneath the foundation pit's centerline, giving rise to a unique "n"-shaped protrusion.

(3) Additionally, as the stiffness of the foundation soil and the depth of the tunnel increase, the resultant deformation in the underlying tunnel experiences a gradual reduction, albeit at a diminishing rate. Conversely, an escalation in the length and width of the foundation pit excavation leads to a progressive augmentation in the deformation of the underlying tunnel, although to a lesser extent. Hence, during the foundation pit's construction phase, it becomes paramount to curtail excavation-induced disturbances and counteract the resultant deformation's effects on the underlying tunnel.

(4) By taking these factors into careful consideration, the study underscores the imperative of mitigating excavation-linked disturbances and their consequential deformations within the underlying tunnel. This research lends valuable insights into the enhancement of construction methodologies and the adept management of foundation pit excavation's repercussions on the surrounding structures.

## Data Availability

All data included in this study are available upon request by contact with the corresponding author.

## Conflicts of Interest

The authors declare that they have no known competing financial interests or personal relationships that could have appeared to influence the work reported in this paper.

## Authors' Contributions

Y.Q. contributed in conceptualization, methodology, supervision, and project administration. X.T. contributed in methodology, software, data processing, and writing—original draft. Z.H. contributed in validation, formal analysis, and writing—review and editing. M.H. contributed in writing—review and editing. All authors have read and agreed to the published version of the manuscript.

## Acknowledgments

The authors thank the Advanced Research Center, Central South University, for providing the experiment conditions. This work was supported by the Hunan Provincial Education Department Foundation under grant number 21C0681 and Natural Science Foundation of Hunan Province under grant number 2022JJ50281.

## References

[1] H.-S. Deng, H.-L. Fu, Y. Shi, Y.-Y. Zhao, and W.-Z. Hou, "Countermeasures against large deformation of deep-buried soft rock tunnels in areas with high geostress: a case study," *Tunnelling and Underground Space Technology*, vol. 119, Article ID 104238, 2022.

[2] H. Cheng, J. Chen, and G. Chen, "Analysis of ground surface settlement induced by a large EPB shield tunnelling: a case study in Beijing, China," *Environmental Earth Sciences*, vol. 78, Article ID 605, 2019.

[3] T. E. Vorster, A. Klar, K. Soga, and R. J. Mair, "Estimating the effects of tunneling on existing pipelines," *Journal of Geotechnical and Geoenvironmental Engineering*, vol. 131, no. 11, pp. 1399–1410, 2005.

[4] H.-S. Deng, H.-L. Fu, S. Yue, Z. Huang, and Y.-Y. Zhao, "Ground loss model for analyzing shield tunneling-induced surface settlement along curve sections," *Tunnelling and Underground Space Technology*, vol. 119, Article ID 104250, 2022.

[5] Z. Zhang, M. Huang, C. Zhang, K. Jiang, and M. Lu, "Time-domain analyses for pile deformation induced by adjacent excavation considering influences of viscoelastic mechanism," *Tunnelling and Underground Space Technology*, vol. 85, pp. 392–405, 2019.

[6] H. Sun, L. Wang, S. Chen, H. Deng, and J. Zhang, "A precise prediction of tunnel deformation caused by circular foundation pit excavation," *Applied Sciences*, vol. 9, no. 11, Article ID 2275, 2019.

[7] Z.-T. Yu, H.-Y. Wang, W. Wang et al., "Experimental and numerical investigation on the effects of foundation pit excavation on adjacent tunnels in soft soil," *Mathematical*

*Problems in Engineering*, vol. 2021, Article ID 5587857, 11 pages, 2021.

[8] C. Wang, H. Sun, J. Zhang, and Y. Lu, "Influence of foundation pit excavation on tunnels at different locations," *Shock and Vibration*, vol. 2022, Article ID 4282253, 12 pages, 2022.

[9] F. Meng, R. Chen, Y. Xu, H. Wu, and Z. Li, "Centrifuge modeling of effectiveness of protective measures on existing tunnel subjected to nearby excavation," *Tunnelling and Underground Space Technology*, vol. 112, Article ID 103880, 2021.

[10] X. Zhao, H. Wang, Z. Li et al., "Numerical study on the deformation of tunnels by excavation of foundation pit adjacent to the subway," *Applied Sciences*, vol. 12, no. 9, Article ID 4752, 2022.

[11] H. Xu, H. F. Schweiger, and H. Huang, "Influence of deep excavations on nearby existing tunnels," *International Journal of Geomechanics*, vol. 13, no. 2, pp. 170–180, 2013.

[12] J. Shi, Z. Fu, and W. Guo, "Investigation of geometric effects on three-dimensional tunnel deformation mechanisms due to basement excavation," *Computers and Geotechnics*, vol. 106, pp. 108–116, 2019.

[13] H. Deng, H. Fu, Y. Shi, Z. Huang, and Q. Huang, "Analysis of asymmetrical deformation of surface and oblique pipeline caused by shield tunneling along curved section," *Symmetry*, vol. 13, no. 12, Article ID 2396, 2021.

[14] H. Sun, Y. Chen, J. Zhang, and T. Kuang, "Analytical investigation of tunnel deformation caused by circular foundation pit excavation," *Computers and Geotechnics*, vol. 106, pp. 193–198, 2019.

[15] K. Cheng, R. Xu, H. Ying et al., "Analytical method for predicting tunnel heave due to overlying excavation considering spatial effect," *Tunnelling and Underground Space Technology*, vol. 138, Article ID 105169, 2023.

[16] H. Hirai, "Settlements and stresses of multi-layered grounds and improved grounds by equivalent elastic method," *International Journal for Numerical and Analytical Methods in Geomechanics*, vol. 32, no. 5, pp. 523–557, 2008.

[17] Y. Zhuang, X. Cui, and S. Hu, "Numerical simulation and simplified analytical method to evaluate the displacement of adjacent tunnels caused by excavation," *Tunnelling and Underground Space Technology*, vol. 132, Article ID 104879, 2023.

[18] Z. Zhou, Y. Chen, Z. Liu, and L. Miao, "Theoretical prediction model for deformations caused by construction of new tunnels undercrossing existing tunnels based on the equivalent layered method," *Computers and Geotechnics*, vol. 123, Article ID 103565, 2020.

[19] Z. Zhang, M. Zhang, and Q. Zhao, "A simplified analysis for deformation behavior of buried pipelines considering disturbance effects of underground excavation in soft clays," *Arabian Journal of Geosciences*, vol. 8, pp. 7771–7785, 2015.

[20] D.-M. Zhang, Z.-K. Huang, Z.-L. Li, X. Zong, and D.-M. Zhang, "Analytical solution for the response of an existing tunnel to a new tunnel excavation underneath," *Computers and Geotechnics*, vol. 108, pp. 197–211, 2019.

[21] J. Zhang, R. Xie, and H. Zhang, "Mechanical response analysis of the buried pipeline due to adjacent foundation pit excavation," *Tunnelling and Underground Space Technology*, vol. 78, pp. 135–145, 2018.

[22] R. D. Mindlin, "Force at a point in the interior of a semi-infinite solid," *Physics*, vol. 7, pp. 195–202, 1936.

[23] P.-T. Simic-Silva, B. Martínez-Bacas, R. Galindo-Aires, and D. Simic, "3D simulation for tunnelling effects on existing piles," *Computers and Geotechnics*, vol. 124, Article ID 103625, 2020.

[24] H. Tanahashi, "Formulas for an infinitely long Bernoulli–Euler beam on the pasternak model," *Soils and Foundations*, vol. 44, no. 5, pp. 109–118, 2004.

[25] S. Miliziano and A. de Lillis, "Predicted and observed settlements induced by the mechanized tunnel excavation of metro line C near S. Giovanni station in rome," *Tunnelling and Underground Space Technology*, vol. 86, pp. 236–246, 2019.

[26] P. Ni and S. Mangalathu, "Fragility analysis of gray iron pipelines subjected to tunneling induced ground settlement," *Tunnelling and Underground Space Technology*, vol. 76, pp. 133–144, 2018.

[27] R. Liang, T. Xia, Y. Hong, and F. Yu, "Effects of above-crossing tunnelling on the existing shield tunnels," *Tunnelling and Underground Space Technology*, vol. 58, pp. 159–176, 2016.

[28] H. Lai, H. Zheng, R. Chen, Z. Kang, and Y. Liu, "Settlement behaviors of existing tunnel caused by obliquely under-crossing shield tunneling in close proximity with small intersection angle," *Tunnelling and Underground Space Technology*, vol. 97, Article ID 103258, 2020.

[29] R. Hasanpour, J. Schmitt, Y. Ozcelik, and J. Rostami, "Examining the effect of adverse geological conditions on jamming of a single shielded TBM in Uluabat tunnel using numerical modeling," *Journal of Rock Mechanics and Geotechnical Engineering*, vol. 9, no. 6, pp. 1112–1122, 2017.

[30] W.-C. Cheng, Z.-P. Song, W. Tian, and Z.-F. Wang, "Shield tunnel uplift and deformation characterisation: a case study from Zhengzhou metro," *Tunnelling and Underground Space Technology*, vol. 79, pp. 83–95, 2018.

[31] H. Cheng, R. Chen, H. Wu, F. Meng, and Y. Yi, "General solutions for the longitudinal deformation of shield tunnels with multiple discontinuities in strata," *Tunnelling and Underground Space Technology*, vol. 107, Article ID 103652, 2021.